Thermal Expansion and Temperature Dependence of Elastic Moduli of Aromatic Polyamides

Daniel J. Lacks† and Gregory C. Rutledge*

Department of Chemical Engineering, Massachusetts Institute of Technology, Cambridge, Massachusetts 02139

Received June 22, 1994®

ABSTRACT: Finite temperature simulations of the crystalline phase of the aromatic polyamides poly(*p*-phenyleneteraphthalamide) (PPTA) and poly(*p*-benzamide) (PBA) are carried out self-consistently using a molecular mechanics force field for the interatomic potential and quasi-harmonic lattice dynamics for the vibrational free energy. The calculated thermal expansion coefficients agree well with the experimental values. The negative axial thermal expansion in these aramides is attributed to elastic coupling to the transverse thermal stresses and to a lesser extent to an increase in entropy associated with contraction. The decrease in the axial Young's moduli with temperature is due mainly to effects of the transverse thermal expansion, which decrease the axial Young's moduli by increasing the unstrained volume and moving the system to a region of the potential energy surface with lower curvature. The negative axial thermal expansion and the decrease in axial Young's modulus with temperature are found to be greater in magnitude for PBA than for PPTA, in agreement with experiment.

I. Introduction

High-performance materials composed of highly crystalline polymers are extensively used because of their high stiffness and strength combined with light weight. Aromatic polyamide fibers, such as Kevlar fiber, which consists of poly(*p*-phenyleneteraphthalamide), are the most commonly used polymers for this purpose. Although there has been much success in explaining general aspects of the structural and elastic properties of polymer crystals in terms of the molecular architecture,[1] a similar clarification of the temperature dependence of these properties has been lacking. As these materials find wider applications and more demand is placed on their ultimate properties, an understanding of the temperature dependence of these properties will be necessary to avoid material failure.

The thermal expansion and the temperature dependence of the elastic moduli are intimately related and must be considered together. The isothermal stiffness moduli, C^{T}_{ij} (using Voigt notation), can be defined by[2]

$$C^{T}_{ij} = \frac{1}{V_T}\left[\frac{\partial^2 A}{\partial\epsilon_i\partial\epsilon_j}\right]_{T,\epsilon_{k\neq i,j}} \tag{1a}$$

$$= \frac{1}{V_T}\left[\frac{\partial^2 U_{pot}}{\partial\epsilon_i\partial\epsilon_j}\right]_{T,\epsilon_{k\neq i,j}} + \frac{1}{V_T}\left[\frac{\partial^2 U_{vib}}{\partial\epsilon_i\partial\epsilon_j}\right]_{T,\epsilon_{k\neq i,j}} - \frac{T}{V_T}\left[\frac{\partial^2 S}{\partial\epsilon_i\partial\epsilon_j}\right]_{T,\epsilon_{k\neq i,j}} \tag{1b}$$

where A is the Helmholtz free energy, U_{pot} is the potential energy, U_{vib} is the vibrational energy, S is the entropy, T is the temperature, V_T is the unstrained volume at temperature T, and ϵ_j is the j component of the strain. Aside from the explicit temperature dependence of the C^{T}_{ij} due to the entropic term, temperature dependences of the C^{T}_{ij} also arise from the temperature dependence of the quantum mechanical vibrational energy and entropy and from thermal expansion, which changes both the unstrained volume V_T and the local shape of the potential energy surface (by changing the reference state at which the second derivatives are taken). Thermal expansion significantly affects the magnitudes of the elastic moduli and therefore must be considered in addition to entropic effects.[3]

Conversely, the thermal expansion coefficients, α_i, depend on the elastic moduli according to the relation:[2]

$$\alpha_i = \frac{C_v}{V}\sum_{j=1}^{6}\gamma_j S^{T}_{ij} \tag{2}$$

where C_v is the heat capacity at constant volume and S^{T}_{ij} is the isothermal compliance modulus (related to the stiffness modulus by $\mathbf{S} = \mathbf{C}^{-1}$). The Gruneisen parameter, γ_i, is related to the change in entropy with strain,[2]

$$\gamma_i = \frac{1}{C_v}\frac{\partial S}{\partial\epsilon_i} \tag{3}$$

Since α_i is a strain per degree of temperature, the quantity $(C_v/V)\gamma_j$ represents a thermally induced stress per degree of temperature. The thermal expansion along an axis can then be considered as the elastic response to the thermal stress along that axis, plus the elastic response to the thermal stresses along the other axes. Thus thermal expansion along one axis cannot be fully explained without considering the thermal effects along the other axes.

Most previous examinations of the temperature dependence of the elastic moduli of polymer crystals neglected either thermal expansion or entropic effects. For example, the lattice dynamics calculations of Tashiro[1] and Tashiro *et al.*[4] and the continuum theory of Ii *et al.*[5] did not account for thermal expansion, and the static-lattice calculation by Karasawa *et al.*[6] did not include entropic effects. Also, previous studies of axial thermal expansion in polymer crystals did not account for the effects of the thermal stresses in the directions transverse to the chain axis.[5,7,8] We have recently reported the results of our consistent lattice dynamics simulations of the temperature dependence of the properties of polyethylene[9] and isotactic polypropylene,[10] which included both the thermal expansion and entropic effects on the crystal properties. Temperature-dependent properties were de-

† Present address: Department of Chemical Engineering, Tulane University, New Orleans, LA 70118.

® Abstract published in *Advance ACS Abstracts*, October 15, 1994.

0024-9297/94/2227-7197$04.50/0

termined from first principles by minimizing the quantum mechanical free energy of the crystal calculated in the quasi-harmonic approximation. These results were in good agreement with the results of experiments on highly crystalline samples and led to new conclusions regarding the temperature dependence of the elastic moduli of polyethylene and the axial thermal expansion of isotactic polypropylene. In the present paper we apply the same techniques to the aromatic polyamides poly(*p*-phenyleneteraphthalamide) (PPTA) and poly(*p*-benzamide) (PBA).

II. Computational Method

In the present simulations, the forces between atoms are represented by a molecular mechanics force field, and thermal effects are included within the quasi-harmonic approximation. The unit cell volumes are obtained by minimizing the free energy at the specified temperature.

a. **Vibrational Free Energy.** The vibrational free energy and temperature dependence of properties can be efficiently evaluated within the quasi-harmonic approximation (QHA).[11] In the QHA, terms higher than second-order in the Taylor expansion of the potential energy are neglected, and the resulting harmonic potential energy surface and vibrational frequencies vary with the lattice parameters. Therefore anharmonic effects due to volume changes are incorporated in the QHA, but the anharmonic coupling of the vibrational modes is neglected. Quantum mechanical effects, which are important for vibrational motion with frequencies $\nu > kT/h$ ($\approx$200 cm^{-1} at room temperature), are included in the present calculations.

The quasi-harmonic vibrational free energy, A_{vib}, at a temperature T is given quantum mechanically by

$$A_{vib} = \frac{\int_{BZ} d\mathbf{k} \sum_{i}^{3N_u} {}^1/_2 \hbar\omega_i(\mathbf{k}) + kT \ln\left(1 - \exp\left[\frac{-\hbar\omega_i(\mathbf{k})}{kT}\right]\right)}{\int_{BZ} d\mathbf{k}} \quad (4)$$

where $\mathbf{k}$ is a wavevector, $\omega_i(\mathbf{k})$ is the vibrational frequency of mode i for wavevector $\mathbf{k}$, N_u is the number of atoms in the unit cell, and the integrals over BZ are integrals over the Brillouin zone. The quasi-harmonic heat capacity at constant volume, C_v, is given by

$$C_v = \frac{\int_{BZ} d\mathbf{k} \sum_{i}^{3N_u} C_v[\omega_i(\mathbf{k})]}{\int_{BZ} d\mathbf{k}} \quad (5a)$$

$$C_v(\omega) = \frac{k\left(\frac{\hbar\omega}{kT}\right)^2 \exp\left(\frac{\hbar\omega}{kT}\right)}{\left[\exp\left(\frac{\hbar\omega}{kT}\right) - 1\right]^2} \quad (5b)$$

where the ω in eq 5b takes on the values $\omega_i(\mathbf{k})$. The entropy, S, can be calculated by

$$S = -\frac{1}{T}(A_{vib} - E_{vib}) \quad (6)$$

where E_{vib} is the vibrational energy,

$$E_{vib} = \frac{\int_{BZ} d\mathbf{k} \sum_{i}^{3N_u} {}^1/_2 \hbar\omega_i(\mathbf{k}) + \hbar\omega_i(\mathbf{k})\left[\exp\left[\frac{\hbar\omega_i(\mathbf{k})}{kT}\right] - 1\right]^{-1}}{\int_{BZ} d\mathbf{k}} \quad (7)$$

The elastic moduli and Gruneisen parameters were obtained from eq 1 and 3 by calculating the derivatives with respect to strain numerically.

The equation of state was determined by minimizing the quasi-harmonic free energy with respect to unit cell lattice parameters. This method has previously been applied to ionic crystals,[12] minerals,[13] zeolites,[14] metal alloys,[15] and polymer crystals.[9,10] We examined the accuracy of this method elsewhere by comparing the results to exact results obtained by Monte Carlo simulation and found that properties are accurately calculated up to half to two-thirds of the melting temperature for the Lennard-Jones solid.[16]

The equilibrium structures at a given temperature were obtained as follows: For a given set of lattice parameters, the potential energy is minimized with respect to the variables describing the atomic positions in the unit cell, using an analytical first derivative technique.[17] After minimization of these internal coordinates, the numerical integration of the vibrational free energy over the Brillouin zone is carried out: for each integration point, analytical second derivatives of the energy, and from these the vibrational frequencies and the vibrational free energy, are calculated. Gauss–Legendre quadrature with 24 integration points is used to carry out the Brillouin zone integrations. The total Gibbs free energy is obtained as the sum of the potential energy and the vibrational free energy for this set of lattice parameters. The lattice parameters which yield the minimum Gibbs free energy are the equilibrium lattice parameters.

b. **Force Field.** The PCFF force field[18] was used for the present simulations. The partial atomic charges were computed using the bond increment method as implemented in the PCFF force field, with the modification of setting the bond increment parameters to zero for the $C_{carbonyl}$–$C_{aromatic}$, $C_{carbonyl}$–N, and $C_{aromatic}$–N bonds (which is consistent with the CFF91 force field[18]). The modified partial atomic charges are closer to previous estimates of the atomic charges in PPTA derived from semiempirical quantum mechanical calculations[19] and lead to an equilibrium structure in better agreement with experiment. Where indicated, calculations were also carried out with the Dreiding force field,[20] with the purpose of demonstrating that our conclusions are independent, at least qualitatively, of the choice of force field.

In our computer program, the long range Coulombic and dispersion interactions are evaluated with Ewald sum techniques,[11,21] and the repulsive nonbonded interaction is evaluated in a direct space sum. Analytical first and second derivatives of the potential energy with respect to the atomic coordinates are calculated for use in geometry optimizations and the calculation of vibrational frequencies.

c. **Crystal Structures.** The repeat units of PPTA and PBA are shown in Figure 1. The crystal structures investigated here are shown in Figure 2. Structures based on the experimental crystal structures were used as starting points;[22,23] no attempt was made to map out multiple minima in the energy surface as was done previously.[19] Both polymers consist of phenyl rings connected by amide groups but differ in the orientation of every second amide linkage along the chain. The experimentally determined conformations of the amide groups are approximately planar, and the phenyl rings rotate out of the plane of the amide groups by approximately 35°. This angle represents a compromise between the repulsive nonbonded interactions of the amide hydrogen or oxygen with a phenyl hydrogen, which are minimized when the phenyl rings are perpendicular to the plane of the amide groups, and the stabilizing π electron delocalization, which is maximized when the phenyl rings are in the plane of the amide groups. In PPTA the two phenyl rings in the repeat unit are rotated in opposite directions with respect to the amide groups, whereas in PBA the rings are rotated in the same direction.

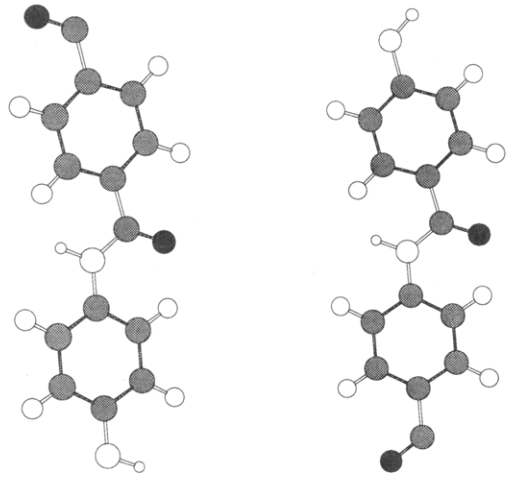

Figure 1. Repeat units of PPTA and PBA. Key: carbon (dark gray), hydrogen (white), oxygen (black), nitrogen (light gray).

Hydrogen bonding occurs between amide groups on adjacent chains along the *b* axis. The PBA crystal lattice is orthorhombic, and the PPTA lattice is monoclinic, but with the nonorthogonal angle between the *a* and *b* axes differing only slightly from 90°.

III. Results

The equilibrium lattice parameters as a function of temperature for PPTA and PBA are shown in Figure 3. The calculated volumes are somewhat larger than the experimental values because the nonbonded force field parameters were obtained by fitting static-lattice structures to experimental data taken at room temperature (some effects of both zero-point and thermal vibrational motion are implicitly included in the nonbonded potential parameters). The results for the average thermal expansion between 300 and 500 K are given in Table 1 and compared with the experimental results of Ii *et al.*[24] In agreement with experimental results, thermal expansion is smaller along the *b* axis than along the *a* axis, and the thermal expansion is negative along the *c* axis (i.e., $\alpha_a > \alpha_b > 0 > \alpha_c$).

The calculated Young's moduli E_i (defined as the inverses of the diagonal compliance moduli, $E_i = 1/S^{T}_{ii}$, $i = 1, 2, 3$) are shown as functions of temperature in Figure 4. The Young's modulus is largest along the chain direction due to the strong intramolecular bonds and is larger along the *b* axis than along the *a* axis because of the hydrogen bonds parallel to the *b* axis; similar results were reported in previous static-lattice calculations.[25,26] The calculated E_3 at room temperature of 273 GPa for PPTA is higher than the experimentally reported values of 150–240.[27-31] All of the Young's moduli are found to be greater for PPTA than for PBA, over the whole range of temperatures. The larger E_3 for PPTA as compared to PBA disagrees with the available experimental results,[27] although it agrees with previous calculations.[26,37] As noted by other investigators,[37] an all-trans conformation for PBA would exhibit a large E_3, in accord with the experimental record; however, this conformation appears to be inconsistent with the X-ray data.

For both PPTA and PBA, E_2 and E_3 are found to decrease significantly with temperature, while the temperature dependence of E_1 is relatively small. The calculated E_3 decreases between 300 and 500 K by approximately 0.07 GPa/K for PPTA and 0.13 GPa/K for PBA, as compared to the experimental results of 0.12 GPa/K for PPTA and 0.21 GPa/K for PBA.[27] Although the calculated changes in E_3 with temperature are significantly smaller than those observed experimentally, we note that the changes in the experimental E_3 with temperature may also be influenced by factors such as changes in crystallinity and crystallite orientation with temperature.

The complete set of elastic moduli are given in Table 2. The precision of these values is approximately ±1 GPa, due to the error arising from numerical evaluation of the second derivative in eq 1; this imprecision limits the analysis of the elastic moduli with small temperature dependences. The calculated elastic stiffness matrix is in substantial agreement with previous static lattice calculations: the average rms deviation between the elements of the present stiffness matrix (at $T = 0$) and that of Yang and Hsu[26] is 11 GPa, and the rms deviation from the stiffness matrix of Rutledge and Suter (structure 3 of that paper)[25] is 14 GPa. The C^{T}_{12} stiffness moduli decrease with temperature for both PBA and PPTA, while the C^{T}_{13} and C^{T}_{23} moduli increase with temperature for PBA and remain approximately constant with temperature for PPTA.

The Gruneisen parameters for PPTA and PBA are shown in Figure 5. The Gruneisen parameters along the *a* and *b* axes positive and are nearly equal for PPTA and PBA. The Gruneisen parameter along the *c* axis, γ_3, is negative over the entire temperature range, indicating that the entropy increases with contraction; γ_3 is significantly larger in magnitude for PBA than for PPTA.

IV. Discussion

a. Thermal Expansion. 1. Axial Thermal Expansion. Negative axial thermal expansion has been observed experimentally in PPTA and PBA.[24,27] The explanation previously given for this thermal contraction is that the contraction allows increased vibrational motion transverse to the chain axis while maintaining (approximately) constant bond lengths, or equivalently that the entropy increases with axial contraction because of a decrease in the frequencies of the transverse vibrational motion.[5] In terms of eq 2, this mechanism implies that $\gamma_3 < 0$ and the $j = 3$ term leads to the observed α_3.[5] This mechanism is the commonly proposed explanation for negative axial thermal contraction in other polymer crystals.[7,8,32-35] Our previous simulation results for negative axial thermal expansion in polyethylene are also in agreement with this mechanism.[9]

However, negative axial thermal expansion can also be due to an elastic response to the thermal stresses in the directions transverse to the chain axis, i.e., the terms $\gamma_1 S^{T}_{13}$ and $\gamma_2 S^{T}_{23}$ in eq 2.[36] We have previously shown that it is this effect which leads to the axial thermal contraction in isotactic polypropylene; the entropy increases with axial expansion for isotactic polypropylene, which alone would lead to *positive* axial thermal expansion.[10] Therefore, the mechanism in which the negative axial thermal expansion in polymer crystals is due to an increase in entropy associated with contraction does not appear to be "universal".[35] The elastic response to transverse thermal stresses must be considered in an objective analysis of the axial thermal expansion of polymer crystals.

We therefore subdivide our results for the axial thermal expansion of PPTA and PBA into contributions from thermal effects both along and transverse to the chain axis. These results are presented in Table 3. As noted above, both PPTA and PBA have negative axial (i.e.,

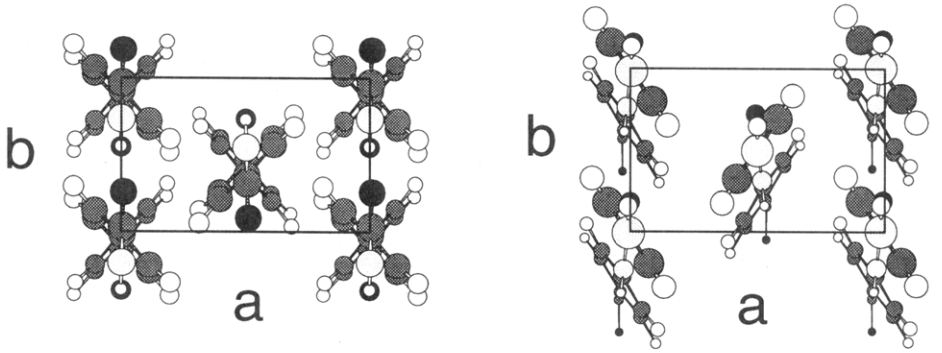

Figure 2. (a, left) Crystal structure of PPTA (modification 1); (b, right) crystal structure of PBA. Key: carbon (dark gray), hydrogen (white), oxygen (black), nitrogen (light gray). Based on structures from ref 23.

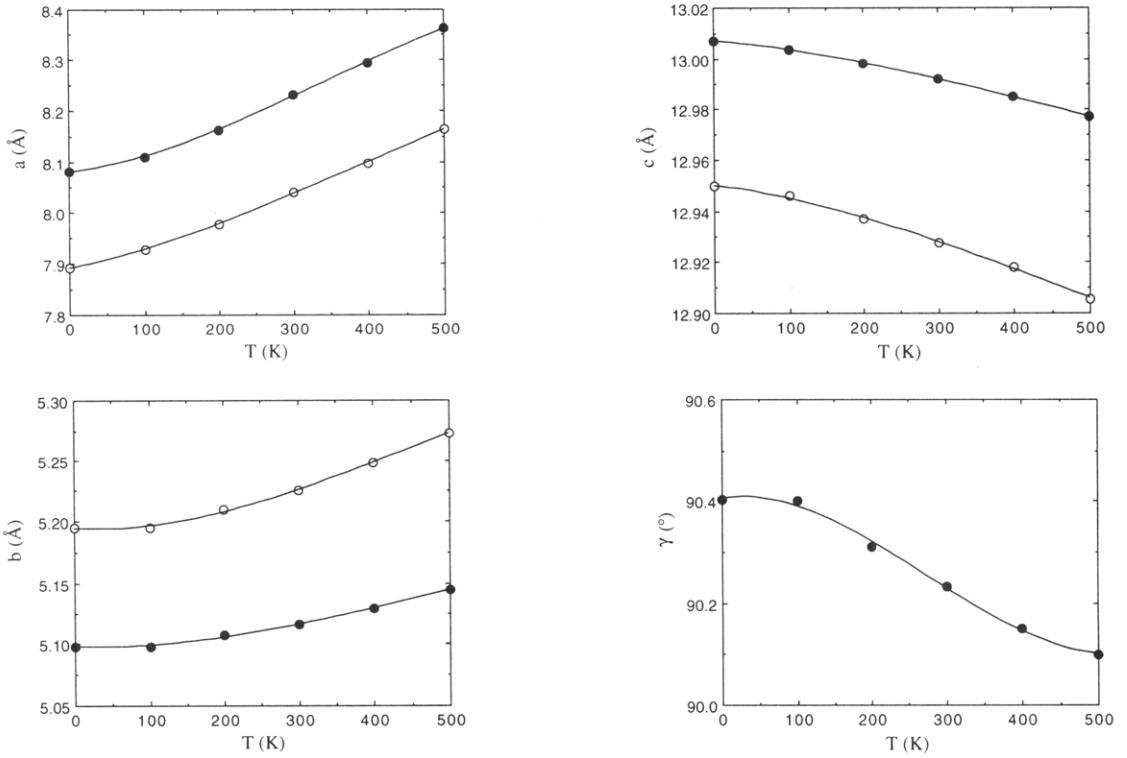

Figure 3. Lattice parameters as a function of temperature. Filled symbols are PPTA, open symbols are PBA. For PBA, the angle γ is always 90°. The experimental room temperature results for PPTA are a = 7.80 Å, b = 5.19 Å, c = 12.9 Å, γ = 90° and for PBA are a = 7.71 Å, b = 5.14 Å, c = 12.8 Å.[23]

Table 1. Average Thermal Expansion between 300 and 500 K

	PPTA		PBA	
	calculated	experimental[a]	calculated	experimental[a]
α_1 (10^{-5} K^{-1})	7.9	8.3	7.7	7.0
α_2 (10^{-5} K^{-1})	2.9	4.7	4.6	4.1
α_3 (10^{-5} K^{-1})	−0.57	−0.29	−0.84	−0.77

[a] Ii *et al.*, ref 24.

parallel to the chain axis) Gruneisen parameters, which contribute to axial thermal contraction as had previously been suggested.[5] However, the dominant contribution to axial thermal contraction is the elastic response to the transverse thermal stresses, which leads to 80% of the total axial thermal contraction in both PPTA and PBA. Previous analyses which assumed that the terms $\gamma_i S^T_{i3}$ ($i \neq 3$) are insignificant[5] should be reconsidered.

The importance of the elastic coupling on the axial thermal contraction is further demonstrated by calculations which show that in response to changes in the a and b lattice parameters, elastic coupling due to potential energy effects alone causes the c lattice parameter to change significantly. Two sets of static-lattice calculations on PPTA were carried out in which the lattice parameters a and b were fixed at their calculated equilibrium values for 300 and 500 K, while the lattice parameter c (as well as all atomic positions) was varied to minimize the *potential* energy. The lattice parameter c which gives the minimum potential energy was found to decrease in going from the equilibrium a and b parameters at 300 K to the equilibrium a and b parameters at 500 K, by an amount corresponding to a thermal expansion of -0.34×10^{-5} K^{-1}. This calculation was also carried out with the Dreiding force field, which led to an effective thermal expansion of -0.55×10^{-5} K^{-1}. We therefore believe that the importance of the elastic coupling in the axial thermal contraction of PPTA is not an artifact of the PCFF force field.

The magnitude of the axial thermal contraction, α_3, is larger in PBA than in PPTA because of both a larger axial contraction due to the associated entropy increase and greater elastic coupling to the transverse thermal stress. The axial contraction due to the associated entropy increase is larger for PBA than for PPTA primarily because the entropy increase is larger for PBA (at 400 K, γ_3(PBA)

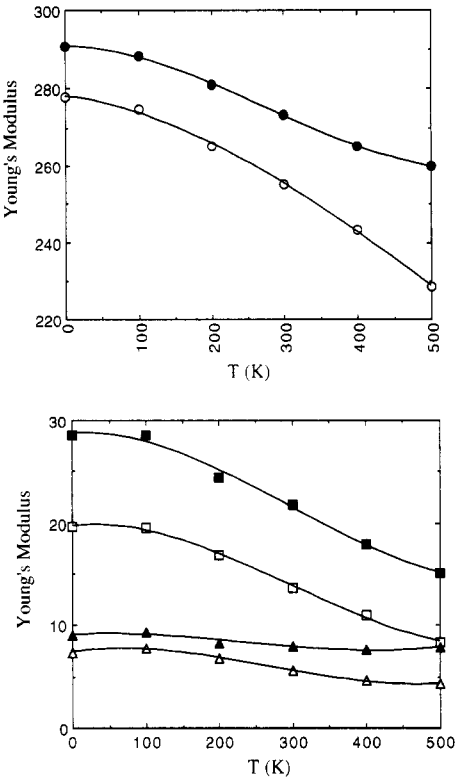

Figure 4. Young's moduli as a function of temperature. Filled symbols are PPTA, open symbols are PBA; triangles are E_1, squares are E_2, and circles are E_3.

Table 2. Isothermal Elastic Stiffness Constants[a]

	0 K	100 K	200 K	300 K	400 K	500 K
			PPTA			
C^T_{11}	13.3	13.5	12.4	11.9	11.8	12.1
C^T_{22}	41.6	40.7	36.1	32.2	27.6	23.4
C^T_{33}	300.1	297.4	290.6	283.7	276.5	271.8
C^T_{44}	14.7	15.1	14.4	14.3	14.1	14.5
C^T_{55}	0.1	1.0	0.1	0.5	0.1	1.0
C^T_{66}	6.1	6.7	6.1	6.1	5.7	8.1
C^T_{12}	13.1	12.8	12.0	11.1	10.6	9.9
C^T_{13}	10.9	10.9	10.6	10.5	10.7	10.8
C^T_{23}	14.5	14.5	14.3	14.2	14.5	14.8
			PBA			
C^T_{11}	12.4	12.6	11.4	10.1	9.1	8.7
C^T_{22}	33.0	31.6	28.5	24.6	21.4	17.1
C^T_{33}	287.3	284.0	276.4	267.9	258.2	246.4
C^T_{44}	22.9	22.6	21.7	19.0	16.4	14.3
C^T_{55}	0.2	0.9	1.7	0.7	0.2	0.2
C^T_{66}	6.9	7.6	7.5	6.2	5.7	5.1
C^T_{12}	12.8	12.3	11.4	10.5	9.7	8.7
C^T_{13}	10.3	10.2	10.4	10.5	11.0	11.0
C^T_{23}	14.7	15.0	15.3	15.6	15.9	16.5

[a] The off-diagonal elements C^T_{4x}, C^T_{5x}, and C^T_{6x} were all found to be less than 1 GPa for PPTA and are equal to zero by symmetry for PBA. The precision of these results is approximately ±1 GPa.

= −0.4 and γ_3(PPTA) = −0.16), but also because S^T_{33} is larger for PBA (see Figure 4, which shows $E_3 = 1/S^T_{33}$). The axial contraction due to the elastic coupling to the transverse thermal stresses is larger for PBA than for PPTA because the off-diagonal compliance moduli are larger for PBA, while the transverse thermal stresses are similar in magnitude for the two polymers.

2. Transverse Thermal Expansion. The thermal expansion is smaller along the *b* axis than along the *a* axis because the hydrogen bonding between amide groups on adjacent chains along the *b* axis leads to S^T_{22} being significantly less than S^T_{11}.

Simulation and experiment agree in the result that thermal expansion along the *a* axis, α_1, is slightly greater

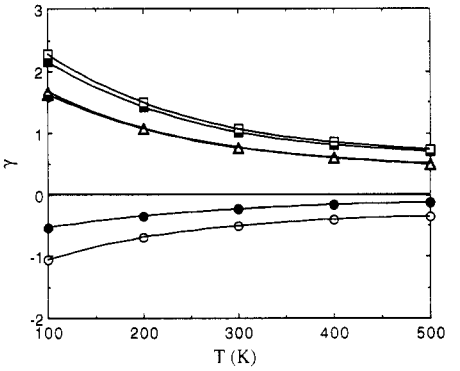

Figure 5. Gruneisen parameters as a function of temperature. Filled symbols are PPTA, open symbols are PBA; triangles are E_1, squares are E_2, and circles are E_3.

Table 3. Component Contributions to Axial Thermal Expansion of PPTA and PBA, at T = 400 K

	$\alpha_3 = (C_v/V)\sum_{j=1}^{3}\gamma_j S^T_{3j}$	$(C_v/V)[\gamma_1 S^T_{13} + \gamma_2 S^T_{23}]$	$(C_v/V)\,\gamma_3 S^T_{33}$
PPTA (10^{-5} K^{-1})	−0.54	−0.43	−0.11
PBA (10^{-5} K^{-1})	−0.94	−0.63	−0.31

in PPTA than in PBA. The simulations find the *b* axis thermal expansion, α_2, to be greater for PBA than for PPTA; this result is due to S^T_{22} being larger for PBA than for PPTA (see Figure 4, which shows $E_2 = 1/S^T_{22}$). The experimental investigation, in contrast, reports that α_2 is larger for PPTA.[24] This discrepancy may be due to approximations in either the experimental analysis or the present calculations. In the experimental investigation, Ii *et al.* used X-ray measurements to obtain the lattice parameter *b* based on the assumption of a pseudo-orthohombic lattice, which is exact when the crystallographic angle $\gamma = 90°$. The angle γ is close to 90°,[22,23] and the errors in *b* due to the pseudo-orthorhombic assumption are small relative to *b*. However, since the *changes* in *b* with temperature are small, the errors resulting from the neglect of changes in γ with temperature may be significant for α_2. Our calculations suggest that γ will change by approximately 0.2° in going from 300 to 500 K; even such a small change in γ with temperature can lead to errors in pseudo-orthorhombic estimations of α_2 which are comparable in magnitude to the reported experimental differences in α_2 between PPTA and PBA (refer to Table 2). We note also that at higher temperatures (500–700 K), Ii *et al.* find α_2 to be larger for PBA than for PPTA.[24] Another possible source of the discrepancy may be the approximate nature of the force field itself. In particular, the room temperature *b* lattice parameter is underestimated for PPTA and overestimated for PBA. While the errors in the equilibrium *b* lattice parameters are small (<1.5%), because S^T_{22} increases with *b* the sign of these errors would account for underestimation of α_2 in PPTA and overestimation of α_2 in PBA (from eq 2).

b. Temperature Dependence of Elastic Moduli. 1. Axial Stiffness Modulus. As discussed in the Introduction, temperature dependences of C^T_{ij} arise not only from the entropic contribution to the free energy, but also as a consequence of thermal expansion, which affects C^T_{ij} through changes in the unstrained volume V and the values of the second derivative of the potential energy, vibrational energy, and entropy. The contribution to C^T_{33} due to potential energy alone (i.e., the first term in eq 1b, which includes both intra- and intermolecular interactions), abbreviated here as C^T_{33}(PotE) is compared to the total C^T_{33} (including both potential energy and vibrational free energy effects) for PPTA in Figure 6; the effects of the

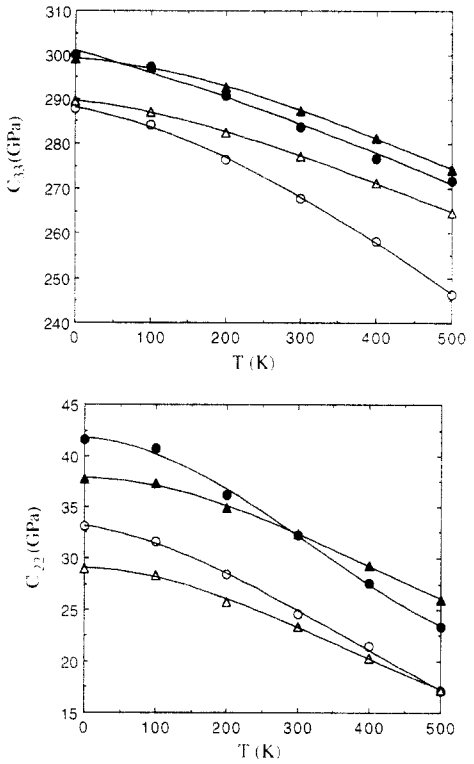

Figure 6. Comparison of C^T_{ii}(PotE) to C^T_{ii}. (a, top) C^T_{33}(PotE) vs C^T_{33}; PPTA (filled symbols), PBA (open symbols). (b, bottom) C^T_{22}(PotE) vs C^T_{22}; symbols same as in a. The effects that contribute to C_{Tii}, other than the potential energy, are the zero-point vibrational energy and the entropic term in the free energy. These effects can, in general, lead to C^T_{ii} being either greater or less than C^T_{ii}(PotE).

vibrational motion on the magnitude of C^T_{33} in these materials are found to be much less than previously estimated.[25] Approximately 80% of the decrease in C^T_{33} from 300 to 400 K is due to the effects of thermal expansion on the potential energy contribution, of which half is from the increase in volume and half is from a decrease in the value of the second derivative of the potential energy. In general, the vibrational contribution to C^T_{33} (i.e., C^T_{33}(PotE)) contains two contributions arising from the vibrational energy U_{vib} and entropy S (eq 1b). The first contribution, $\partial^2 U_{vib}/\partial\epsilon_3^2$, can lead to either an increase (as in PPTA) or a decrease (as in PBA) in C^T_{33} with respect to C^T_{33}(PotE) at low temperature, but this effect necessarily falls to zero at higher temperatures, since the vibrational energy is frequency-independent in the classical limit. The second contribution, $-T\partial^2 S/\partial\epsilon_3^2$, leads to a decrease in C^T_{33} with respect to C^T_{33}(PotE) which is zero at T = 0 K and increases in magnitude with increasing temperature. These effects are seen in Figure 6a.

The decrease in the value of the second derivative of the potential energy as the volume expands (i.e., as the polymer chains move farther apart) is related to the observations from previous static-lattice calculations that the axial elastic modulus of the PPTA or PBA crystal is significantly larger than that of the corresponding single chain. (The single chain axial elastic modulus is defined using the same volume as for the crystal modulus, and any difference from the crystal axial elastic modulus is due only to the second derivative of the potential energy.[25,26]) Previous calculations are in agreement that an axial deformation in a single chain involves a larger change in torsional energy and a smaller change in van der Waals energy than an equivalent deformation in the crystal. We have carried out further calculations to rationalize this difference in the energetics of the single chain and crystal axial deformations and found that the difference arises from a coupling between the phenyl ring rotation angles and the amide bond angles (i.e., C_{phenyl}–C_{amide}–N and C_{phenyl}–N–C_{amide}). As discussed above, although the stabilization associated with delocalized π bonding is maximized when the phenyl rings are in the plane of the amide groups, the phenyl rings are rotated out of this plane in order to decrease the repulsive nonbonded interactions between a phenyl hydrogen and an amide oxygen or hydrogen (see Figure 1); the resulting phenyl ring rotation angle of approximately 35° represents a compromise between these two opposing effects. However, if an amide bond angle is increased, the phenyl hydrogen and the amide oxygen or hydrogen are moved further apart and the nonbonded repulsion is reduced; the phenyl ring rotation angle will therefore decrease to enhance the delocalized π bonding. Conversely, if an amide bond angle is decreased, the phenyl ring rotation angle will increase due to the increased nonbonded repulsions. Since the PPTA and PBA chains deform axially primarily through changes in the amide bond angles,[37] the relaxation of the phenyl ring rotation angles in response to these bond angle changes will moderate the increase in energy associated with the deformation, thereby decreasing the axial elastic modulus (specifically, the second derivative of the potential energy) relative to that in which the phenyl ring rotation angle is fixed. The PPTA and PBA crystals have higher axial elastic moduli than the corresponding single chains because the phenyl rings are "locked" in place by the surrounding chains within the crystal and cannot rotate in response to changes in the amide bond angles. This effect was observed with both the PCFF and Dreiding force fields.

With thermal expansion the polymer chains move further apart at higher temperatures and the crystal becomes more like a collection of single chains. Therefore, thermal expansion in PPTA and PBA leads to the phenyl rings being able to rotate more freely, with an associated decrease in the second derivative of the potential energy. We note that such a change in the value of the second derivative of the potential energy when the polymer chains move farther apart does not occur for all polymers: previous calculations for polyethylene found the crystal and single chain axial elastic moduli to be very similar.[6]

The larger decrease in C^T_{33} with temperature for PBA as compared to PPTA can be attributed to the entropic contributions to C^T_{33}. The decrease in C^T_{33} due to thermal expansion effects (predominantly in term 1 of eq 1b) is essentially the same as in PPTA and PBA, while the decrease due to the entropic contributions to C^T_{33} (term 3 in eq 1b) is twice as large in PBA.

2. Transverse Stiffness Moduli. The transverse stiffness moduli, C^T_{11} and C^T_{22} were found to decrease with temperature, the decrease for C^T_{22} being larger than for C^T_{11}. A decrease in these elastic moduli would be expected based on potential energy effects alone because the interchain interactions decrease as the polymer chains move further apart. The contribution to C^T_{22} due to potential energy alone, C^T_{22}(PotE), is compared to the total C^T_{22} for PPTA in Figure 6. In this case 70% of the decrease in elastic modulus from 300 to 400 K is due to the effects of thermal expansion on the potential energy contribution, of which 90% results from a decrease in the value of the second derivative of the potential energy and only 10% from the increase in volume. The smaller effect of the volume increase on C^T_{22} as compared to C^T_{33} is due to the smaller magnitude of C^T_{22}—an increase in volume leads to a decrease in elastic modulus which is proportional

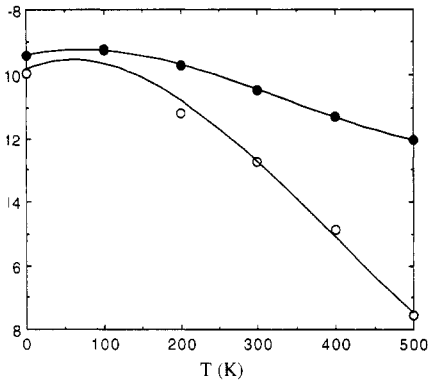

Figure 7. Difference between E_3 and C^T_{33}. Filled symbols are PPTA; open symbols are PBA.

to the magnitude of the elastic modulus. The temperature dependence of C^T_{22} for PBA is similar to that for PPTA.

3. Off-Diagonal Stiffness Moduli. As with the transverse elastic moduli, the off-diagonal moduli would decrease with temperature based on potential energy effects alone because the interchain interactions decrease as the polymer chains move further apart. For this reason, the C^T_{12} of both PPTA and PBA decrease with temperature. However, the C^T_{13} and C^T_{23} of PBA are found to increase with temperature, as was found previously for polyethylene.[9] The reason for the increase in these elastic moduli with temperature is related to the axial thermal contraction mechanism in which chain contraction is due to an entropy increase caused by the transverse vibrational motion: The increase in entropy with contraction (i.e., the quantity $\partial S/\partial\epsilon_3 < 0$) increases in magnitude as the polymer chains move further apart because the transverse vibrational motion becomes less hindered by the surrounding polymer chains. Therefore, the quantity $\partial^2 S/(\partial\epsilon_3\partial\epsilon_j) < 0$ for $j = 1, 2$, and acts to increase the C^T_{j3}. For this reason, the C^T_{13} and C^T_{23} of PBA increase with temperature. For PPTA, the C^T_{13} and C^T_{23} remain approximately constant with temperature because this effect, which is smaller in PPTA than in PBA (see Table 3), just compensates for the decrease in C^T_{13} and C^T_{23} due to potential energy effects.

4. Shear Moduli. The temperature dependences of the shear moduli (C^T_{ii} i = 4,5,6) are too small to be distinguished from the numerical noise in the calculation (with the exception of C^T_{44} of PBA, which decreases significantly with temperature). As with the transverse and off-diagonal stiffness moduli, a decrease in the shear elastic moduli would be expected based on potential energy effects alone because the interchain interactions decrease as the polymer chains move further apart.

5. Young's Moduli. The Young's moduli E_i, which are exactly equal to the C^T_{ii} (i = 1,2,3) when all of the off-diagonal stiffness moduli C^T_{ij} equal zero, have temperature dependences which are similar to those of the C^T_{ii}; slight differences arise due to the temperature dependences of the nonzero off-diagonal C^T_{ij}. The quantity $E_3 - C^T_{33}$ is shown in Figure 7. The larger temperature dependence of $E_3 - C^T_{33}$ for PBA as compared to PPTA is due to the larger temperature dependence of C^T_{13} and C^T_{23} for PBA, as discussed above. The greater temperature dependence of the E_3 for PBA as compared to PPTA can thus be attributed to larger entropic effects in the diagonal C^T_{33} and the off-diagonal C^T_{13} and C^T_{23} elastic moduli; although the effects of thermal expansion on the potential energy contribution are the dominant causes of the temperature dependence of E_3, the magnitudes of these effects are similar for PPTA and PBA.

V. Conclusions

Calculations of the thermal expansion and temperature dependence of the elastic moduli of PPTA and PBA were carried out from first principles, using molecular mechanics force fields for the interatomic interactions and the quasi-harmonic approximation for the vibrational free energy. The temperature dependent properties reported here follow entirely from self-consistent lattice dynamic calculations under these constraints, without any further assumptions. The results of our calculations for the thermal expansion coefficients are in good agreement with experiment. In both PPTA and PBA, thermal expansion is larger along the *a* axis (between hydrogen bonded sheets) than along the *b* axis (within the hydrogen bonded sheets) and is negative along the *c* axis (along the polymer chain). The calculated decrease with temperature of the axial Young's modulus (shown in Figure 4) is somewhat smaller than that found from X-ray experiments;[27] however, the uncertainties in experimentally determined crystallite elastic moduli for polymer crystals are well-known. For example, for polyethylene the axial elastic modulus determined by different experimental methods varies by 50%;[38] also, Northolt has shown that even slight misalignment of crystallites along the fiber axis significantly reduces the observed elastic modulus.[29,30]

The negative axial thermal expansion for PPTA and PBA is attributed primarily to elastic coupling to the thermal stresses transverse to the chain axis. The increase in entropy associated with chain contraction makes a minor contribution (approximately 25%) to the total negative axial thermal expansion.

The decreases in the axial elastic moduli of PPTA and PBA with temperature are due primarily to effects arising from the thermal expansion transverse to the chain axis—this thermal expansion leads to both an increase in equilibrium volume, which decreases the elastic modulus (the stiffness moduli are the second derivatives of the free energy with strain *per unit volume*), and a decrease in the local curvature of the potential energy surface as the chains move apart; this decrease in the second derivative of the potential energy is attributed to a more complete relaxation of the phenyl ring rotation angle in response to the changes in the amide bond angles accompanying axial strain. The effects of the direct entropic contribution (i.e., second derivative of the entropy with respect to strain) on the temperature dependence of the elastic modulus are smaller in magnitude.

The calculations find that the negative axial thermal expansion and the decrease in the axial Young's modulus with temperature are larger in magnitude for PBA than for PPTA, in agreement with experiment.[24,27] The larger axial thermal contraction for PBA as compared to PPTA is due to both a larger increase in entropy with chain contraction and increased elastic coupling to the transverse thermal stresses. The larger temperature dependence of the axial elastic modulus in PBA is due to the direct entropic contribution to the modulus, since the effects of thermal expansion on the elastic modulus are similar for the two materials.

Arguments may be proposed for the design of composite materials based on the results of the current work. Fiber-reinforced composite materials are often composed of a polymer fiber such as PPTA embedded in an amorphous polymer matrix. With changes in temperature, stresses develop at the ends of the fiber because the fiber undergoes axial thermal contraction while the matrix undergoes thermal expansion;[39] these stresses are believed to be a major cause of material failure.[40] The present results

predict that the development of these stresses could be mitigated by matching the fiber and matrix materials such that α_m, the matrix thermal expansion coefficient, is less than the *transverse* thermal expansion coefficients of the fiber. Under such conditions external stresses from the surrounding matrix would counteract the transverse thermal stresses of the fiber, leading to a reduction in the negative axial thermal expansion of the fiber and therefore a reduction in the stress generated at the fiber ends. Also, the present results lead to the prediction that a smaller α_m would reduce the transverse thermal expansion of the fiber and improve the axial stiffness at high temperatures.

Acknowledgment. The authors are grateful to Texaco, Inc. and to E. I. DuPont de Nemours for providing the financial support for this work in the form of the Texaco-Mangelsdorf Chair and a DuPont Young Faculty Award to G.C.R.

References and Notes

(1) Tashiro, K. *Prog. Polym. Sci.* **1993**, *18*, 377.
(2) Weiner, J. H. *Statistical Mechanics of Elasticity*; John Wiley & Sons: New York, 1983.
(3) Leibfried, G.; Ludwig, W. *Solid State Physics*, Seitz, F., Turnbull, D., Ed.; Academic Press: New York, 1961; Vol. 12, p 275.
(4) Tashiro, K.; Kobayashi, M.; Tadokoro, H. *Polym. J.* **1992**, *24*, 899.
(5) Ii, T.; Tashiro, K.; Kobayashi, M.; Tadokoro, H. *Macromolecules* **1987**, *20*, 552.
(6) Karasawa, N.; Dasgupta, S.; Goddard, W. A. *J. Phys. Chem.* **1991**, *95*, 2260.
(7) Chen, F. C.; Choy, C. L.; Young, K. *J. Polym. Sci.: Polym. Phys. Ed.* **1980**, *18*, 2313. Chen, F. C.; Choy, C. L.; Wong, S. P.; Young, K. *J. Polym. Sci.: Polym. Phys. Ed.* **1981**, *19*, 971.
(8) Baughman, R. H. *J. Chem. Phys.* **1973**, *58*, 2976.
(9) Lacks, D. J.; Rutledge, G. C. *J. Phys. Chem.* **1994**, *98*, 1222.
(10) Lacks, D. J.; Rutledge, G. C. *Chem. Eng. Sci.* **1994**, *49* (17), 2881.
(11) Born, M.; Huang, K. *Dynamical Theory of Crystal Lattices*; Oxford University Press: Oxford, 1954. Venkataraman, G.; Feldkamp, L. A.; Sahni, V. C. *Dynamics of Perfect Crystals*; MIT Press: Cambridge, 1975.
(12) Boyer, L. L. *Phys. Rev. B* **1981**, *23*, 3673. Hemley, R. J.; Gordon, R. G. *J. Geophys. Res.* **1985**, *90*, 7803.
(13) Catti, M.; Pavese, A.; Price, G. D. *Phys. Chem. Minerals* **1993**, *19*, 472. Isaak, D. G.; Cohen, R. E.; Mehl, M. J. *J. Geophys. Res.* **1900**, *95*, 7055.
(14) Jackson, R. A.; Parker, S. C.; Tschaufeser, P. *Modelling of Structure and Reactivity in Zeolites*; Catlow, C. R. A., Ed.; Academic Press: London, 1992; p 43.
(15) Rubini, S.; Ballone, P. *Phys. Rev. B* **1993**, *48*, 99.
(16) Lacks, D. J.; Rutledge, G. C. *J. Chem. Phys.*, in press.
(17) Press, W. H.; Flannery, B. P.; Teukolsky, S. A.; Vetterling, W. T. *Numerical Recipes: The Art of Scientific Computing*; Cambridge University Press: Cambridge, 1986.
(18) *Discover Software, version 2.3*; Biosym Technologies: San Diego, 1993.
(19) Rutledge, G. C.; Suter, U. W. *Macromolecules* **1991**, *24*, 1921.
(20) Mayo, S. L.; Olafson, B. D.; Goddard, W. A. *J. Phys. Chem.* **1990**, *94*, 8897.
(21) Karasawa, N.; Goddard, W. A. *J. Phys. Chem.* **1989**, *93*, 7320.
(22) Northolt, M. G. *Eur. Polym. J.* **1974**, *10*, 799.
(23) Tadokoro, H. *Structure of Crystalline Polymers*; John Wiley & Sons: New York, 1979.
(24) Ii, T.; Tashiro, K.; Kobayashi, M.; Tadokoro, H. *Macromolecules* **1986**, *19*, 1772.
(25) Rutledge, G. C.; Suter, U. W. *Polymer* **1991**, *32*, 2179.
(26) Yang, X.; Hsu, S. L. *Macromolecules* **1991**, *24*, 6680.
(27) Ii, T.; Tashiro, K.; Kobayashi, M.; Tadokoro, H. *Macromolecules* **1987**, *20*, 347.
(28) Gaymans, R. G.; Tijssen, J.; Harkama, S.; Bantjes, A. *Polymer* **1976**, *17*, 517.
(29) Northolt, M. G. *Polymer* **1980**, *21*, 1199.
(30) Northolt, M. G.; Hout, R. v. d. *Polymer* **1985**, *26*, 310.
(31) Kim, P. K.; Chang, C.; Hsu, S. L. *Polymer* **1986**, *27*, 34.
(32) Choy, C. L.; Nakafuku, C. *J. Polym. Sci.: Polym. Phys. Ed.* **1988**, *26*, 921.
(33) Kobayashi, Y.; Keller, A. *Polymer* **1970**, *11*, 114.
(34) Davis, G. T.; Eby, R. K.; Colson, J. P. *J. Appl. Phys.* **1970**, *41*, 4316.
(35) Choy, C. L. *Developments in Oriented Polymers*; Ward, I. M., Ed.; Applied Science Publishers: London, 1982; Vol. 1, p 121.
(36) Munn, R. W. *J. Phys. C* **1972**, *5*, 535.
(37) Tashiro, K.; Kobayashi, M.; Tadokoro, H. *Macromolecules* **1977**, *10*, 413.
(38) Nakamea, K.; Nishino, T.; Ohkubo, H. *J. Macromol. Sci.-Phys.* **1991**, *B30*, 1. Holliday, L.; White, J. W. *Pure Appl. Chem.* **1971**, *26*, 545.
(39) See, for example: Fan, C. F.; Hsu, S. L. *Macromolecules* **1989**, *22*, 1474.
(40) See, for example: Termonia, Y. *J. Polym. Sci.: Polym. Phys. Ed.* **1994**, *32*, 969.